Time-resolved measurements of the densities of individual frozen hydrometeors and of fresh snowfall

Dhiraj K. Singh[1], Eric R. Pardyjak[1], and Timothy J. Garrett[2]

[1]Department of Mechanical Engineering, University of Utah, Salt Lake City, UT, USA
[2]Department of Atmospheric Sciences, University of Utah, Salt Lake City, UT, USA

Correspondence: Eric R. Pardyjak
(pardyjak@eng.utah.edu)

Abstract. It is a challenge to obtain accurate measurements of the microphysical properties of delicate, structurally complex, frozen and semi-frozen hydrometeors. We present a new technique for the real-time measurement of the density of freshly fallen individual snowflakes. A new thermal-imaging instrument, the Differential Emissivity Imaging Disdrometer (DEID), is shown through laboratory and field experiments to be capable of providing accurate estimates of individual snowflake and bulk-snow hydrometeor density (which can be interpreted as snow-to-liquid ratio or SLR). The method exploits the rate of heat transfer during the melting of a hydrometeor on a heated metal plate, which is a function of the temperature difference between the hotplate surface and the top of the hydrometeor. The product of the melting speed and melting time yields an equivalent particle thickness normal to the hotplate surface, which can then be used in combination with the particle mass and area on the plate to determine a particle density. Uncertainties in estimates of particle density are approximately 4% based on calibrations with laboratory-produced particles made from water and frozen solutions of salt and water, and from field comparisons with both high-resolution imagery of falling snow and traditional snowpack density measurements obtained at 12-hour intervals. For 17 storms, individual particle densities vary from 19 to 495 kg m^{-3} and storm-mean snow densities vary from 40 to 100 kg m^{-3}. We observe probability distribution functions for hydrometeor density that are nearly Gaussian with kurtoses of ≈ 3 and skewnesses of ≈ 0.01.

1 Introduction

Frozen and semi-frozen hydrometeors have a very wide range of porosities (Dunnavan et al., 2019). Determining their particulate densities and bulk snow-to-liquid ratios (SLR) once fallen on the ground is important to a wide range of fields including hydrology (Rango and Martinec, 1995; Sturm et al., 2010), climatology (Dickinson, 1983), remote sensing at wavelengths ranging from the visible to the microwave (Kendra et al., 1994; Kokhanovsky and Zege, 2004; Gergely et al., 2010), and the parameterization of snowflake fall speeds in weather and climate models (Rutledge and Hobbs, 1984; Hong et al., 2004; Fovell and Su, 2007; Alcott and Steenburgh, 2010; Finlon et al., 2019). Because hydrometeor porosity is invisible to most imaging techniques, obtaining accurate snowflake-density estimates has proven to be a significant challenge where even the best estimates have required the use of sophisticated field programs using multiple instruments (Tiira et al., 2016).

Improvements to weather prediction are currently hampered by an inability to assimilate information about ongoing variabil-
ity in frozen and semi-frozen precipitation particles (Rasmussen et al., 2011). Avalanche forecasting in mountainous regions
depends, in part, on knowledge of the the vertical density structure of freshly fallen snow (Morrison et al., 2023), a parameter
that is typically measured at sparse intervals (Schweizer et al., 2011; Proksch et al., 2016) using techniques such as micro-
computed tomography (μCT), or more typically, with manual gravimetric methods (Proksch et al., 2016).

In our previous work, we showed that a new thermal-imaging instrument, the Differential Emissivity Imaging Disdrometer
(DEID), can be used to measure individual hydrometeor density based on the first automated direct measurements of particle
mass in combination with estimates of the particle spherical-equivalent effective diameter, or by using concurrent photographic
imagery of the morphological characteristics of hydrometeors as they fall (Singh et al., 2021; Rees et al., 2021). While the
spherical-particle approach offers the advantage of simplicity, it was found to lead to snowflake density estimates that were
significantly biased low relative to a method that required an added camera system, likely because snowflakes are not in fact
spheres.

Here, we describe a new method for estimating particle-by-particle frozen hydrometeor density that, like the spherical-
particle method, uses only the DEID to measure mass but infers particle volume instead from DEID measurements of

melting time, particle area, and estimates of the rate of heat transfer from the hotplate to the hydrometeor to obtain a
'melting-speed' (MS).

2   DEID measurement techniques for obtaining hydrometeor mass and density

The DEID consists of an infrared camera pointed at the surface of a low-emissivity aluminum hotplate. To quantify hydrometeor
area on the hotplate, the DEID makes use of the contrasting thermal emissivities of water ($\varepsilon > 0.95$) and aluminum ($\varepsilon < 0.1$) at
the same temperature. Owing to the high difference in emissivity, melted hydrometeors with nearly the same thermodynamic
temperature as the heated plate have strongly contrasting radiative temperatures, such that droplets on the heated plate can
be easily discriminated using a thermal camera. The hotplate surface is roughened, which prevents displacement of melted
snowflakes at high wind speeds as demonstrated in wind tunnel experiments with wind speeds varying from 2 to 12 m s^{-1}.

2.1   Particle mass measurement

The DEID methodology for obtaining the mass of a hydrometeor particle has been described previously by Singh et al. (2021),
Rees et al. (2021), Rees and Garrett (2021), and Morrison et al. (2023). Here, we present a concise summary including recent
modifications to the measurement methodology. Briefly, the mass of individual hydrometeors is obtained by considering the
area of each hydrometeor on a heated plate and the temperature difference between the plate and the surface of the melted
liquid particle, which is integrated over time from the point of first impact of the particle onto the plate surface up to the point
of its complete evaporation.

Specifically, the mass m of an individual snowflake is obtained by applying conservation of energy to a control volume
surrounding each hydrometeor on the hotplate. The heat gained by a snowflake from the heated plate is assumed to be equivalent

to the heat required to increase the snowflake's internal energy plus the heat lost during melting and evaporation as described by the following equation

$$mC_{\text{ice}}(T_0 - T_{\text{ice}}) + mL_f + mC_{\text{liq}}(T_p - T_0) + mL_v = \kappa \int_0^{\Delta t_{\text{evap}}} (T_p - T_h(t))A(t)\, dt. \tag{1}$$

Here, m is the mass of an individual frozen hydrometeor, C_{ice} is the specific heat of ice, T_{ice} is initial temperature of a frozen hydrometer, $T_0 = 0°C$, $L_f = 3.34 \times 10^5$ J kg^{-1} is the latent heat of fusion of water, and $L_v = 2.32 \pm 0.02 \times 10^6$ J kg^{-1} is the latent heat of vaporization of water (see Appendix A1), $C_{\text{liq}} = 4.18 \times 10^3$ J kg$^{-1}K^{-1}$ is the specific heat of liquid water, $A(t)$ is the area of each frozen hydrometeor and water droplet at time t, T_p is the surface temperature of the hotplate during evaporation and it is constant with time, and $T_h(t)$ is the temperature of the frozen hydrometeor and/or water droplet at time t on the hotplate. Δt_{evap} is the time required to melt and evaporate a hydrometeor, and κ is an empirical device-specific calibration coefficient (related to the amount of heat that passes through the metal hotplate to individual hydrometeors per unit time through a unit area with a temperature gradient of one degree) determined to be $7.01 \pm 0.01 \times 10^3$ W m^{-2} K^{-1} (equivalent to $(k/d)_{\text{eff}}$ in Singh et al. (2021)), which is independent of particle size and environmental conditions. In Eq. (1), the area of a hydrometer at any time t can be written as $A(t) = A_{ice}(t) + A_{liq}(t)$, where $A_{ice}(t)$ is the unmelted area of a hydrometer at time t and $A_{liq}(t)$ is the melted area of a hydrometer at time t. After substituting $A(t)$ in Eq. (1), Eq. (1) may be re-written as

$$mC_{\text{ice}}(T_0 - T_{\text{ice}}) + mL_f + mC_{\text{liq}}(T_p - T_0) + mL_v = \kappa \int_0^{\Delta t_{\text{melt}}} (T_p - T_{ice}(t))A_{ice}(t)\, dt + \kappa \int_{t_0}^{\Delta t_{\text{evap}}} (T_p - T_{liq}(t))A_{liq}(t)\, dt. \tag{2}$$

Here, $t = 0$ corresponds to when a frozen hydrometeor hits the hotplate and $t = t_0$ is when the thermal camera sees the liquid portion for the first time. t_0 is the time lag between the melting and evaporation start times, respectively, which is about 0.1 s for the laboratory ice particles tested and negligible for snowflakes observed using our typical thermal-camera recording frame rates. Note that the thermal camera can be adjusted to selectively 'see' particles on the hotplate in specific temperature ranges (see section 3). To more easily evaluate Eq. (2), the camera is set to only see hydrometeors on the hotplate after melting. Hence, $A_{ice}(t) = 0$ for $T_h(t) < 0°C$ and $\kappa \int_0^{\Delta t_{\text{melt}}} (T_p - T_h(t))A_{ice}(t)dt = 0$, which is equal to $mC_{\text{ice}}(T_0 - T_{\text{ice}}) + mL_f$. This trick allows us to remove both terms from Eq. (2), which yields

$$m = \frac{\kappa}{C_{\text{liq}}T_p + L_v} \int_{t_0}^{\Delta t_{\text{evap}}} (T_p - T_w(t))A(t)\, dt. \tag{3}$$

Here, the lower integration bound is rest so that $t_0 = 0$ such that Eq. (3) is evaluated for liquid phase only. $T_w(t)$ is the water droplet temperature at time t. Note that the initial and final temperature of all frozen hydrometeors is $T_0 = 0°C$ and T_p, respectively, during evaporation, and more than $\approx 98\%$ of the mass evaporates at the highest temperature ($\approx T_p$). This is illustrated in the time series of the temperature of an evaporating hydrometeor given in Fig. A1. Note that we use the subscripts ice or s to denote frozen hydrometeors (i.e., ice and snowflake, respectively).

Mass estimates were shown in wind-tunnel calibrations to be nearly independent of environmental conditions, including wind speed, relative humidity, and ambient temperature (Singh et al., 2021). Specifically, wind-tunnel experiments with the DEID showed less than 4% variability in mass measurements of hydrometeors for a wide range of wind speeds, relative humidities, and air temperatures (Singh et al., 2021). The reason for the low sensitivity to environmental conditions is that the DEID directly measures the energy required to melt and evaporate a droplet, mL_{eqv}. For example, the heat-transfer rate to a droplet is dependent on parameters such as wind speed through the Reynolds number (Kosky et al., 2013) and the temperature. However, while higher winds may accelerate heat transfer they also diminish the time for completing evaporation. Because it is the product of the heat-transfer rate and evaporation time that determines particle mass, winds play a minor role in the calculation of mass.

2.2 Particle density

Obtaining frozen hydrometeor density from hydrometeor mass requires an estimate of the particle volume while it is in its frozen state. While the DEID can provide an accurate estimate of snowflake mass m and initial snowflake projected area after it impacts the hotplate A_p, it cannot provide a direct measure of a particle's effective thickness in the direction normal to the hotplate h as illustrated in Fig. 1. In its place, we have developed a method for estimating h based on a 'melting speed' v_{melt} such that $h = v_{\text{melt}}\Delta t_{\text{melt}}$, where Δt_{melt} is the time required to melt an individual snowflake. Using these substitutions, the density of a frozen hydrometeor can be written as

$$\rho_{\text{MS}} = \frac{m}{\mathcal{V}_s} = \frac{m}{A_p v_{\text{melt}}\Delta t_{\text{melt}}}, \tag{4}$$

where ρ_{MS} indicates the density computed using the 'melting speed' method and $\mathcal{V}_s$ is the volume of a snowflake estimated as $A_p v_{\text{melt}}\Delta t_{\text{melt}}$.

We propose a method to measure v_{melt} as a function of the temperature difference across a hydrometeor (ΔT_{melt}) – and hence the heat-transfer rate – as illustrated in Fig. 1. During the time it takes to melt a snowflake, Δt_{melt}, a hydrometeor receives a quantity of energy equal to $mL_{\text{ff}} = mC_{ice}(T_0 - T_{ice}) + mL_f$ (that is, the sum of the internal energy per unit mass of a frozen hydrometeor and its latent heat of fusion) from the hotplate, which is independent of the density of a frozen hydrometeor. v_{melt} is associated with conductive heat flux ($\kappa \Delta T_{\text{melt}}$) from the hotplate to the frozen hydrometeors during melting. We hypothesize that v_{melt} is a function of the temperature difference across a hydrometeor (ΔT_{melt}), and we may write v_{melt} as

$$v_{\text{melt}} = c_{\text{melt}}\Delta T_{\text{melt}}, \tag{5}$$

where $\Delta T_{\text{melt}} = \overline{T_p(t) - T_s(t)}$ during the melting process and $T_s(t)$ is the surface temperature of the frozen portion of the particle during melting and c_{melt} is a constant determined experimentally (see section 4.1).

Now, if v_{melt} from Eq. (5) is substituted into Eq. (4), the MS density equation can now be written as

$$\rho_{\text{MS}} = \frac{m}{c_{\text{melt}}A_p\Delta T_{\text{melt}}\Delta t_{\text{melt}}}. \tag{6}$$

The melting parameter Δt_{melt} is quite short for low-density snowflakes, and hence requires high-frequency recording of thermal images resulting in the generation of a tremendous amount of data, which is not convenient for field experiments. In
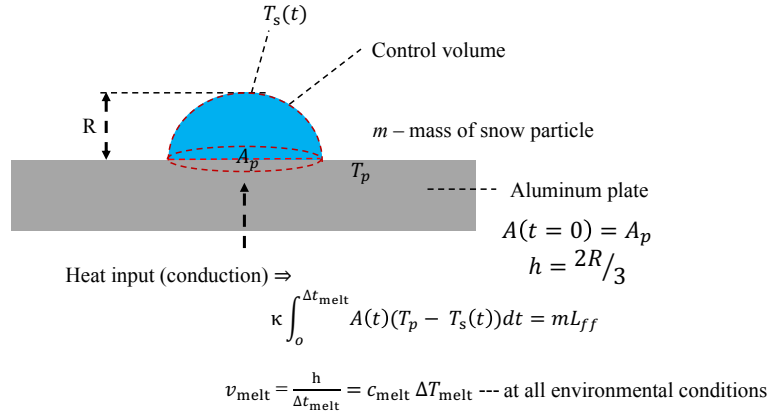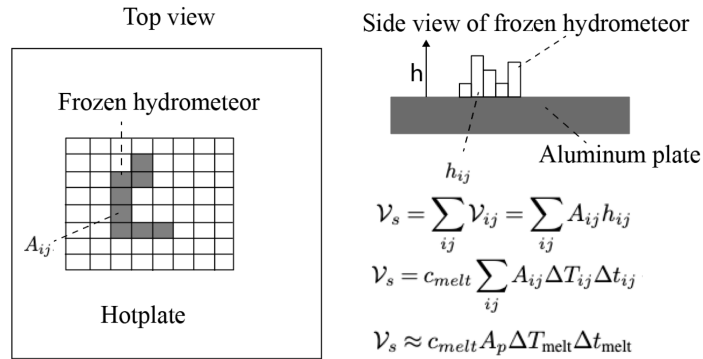
Figure 1. (a) Schematic of the heat transfer process from the DEID's aluminum hotplate to a solid hydrometeor during melting. R and A_p are the radius and base area of the hydrometeor on the hotplate, respectively. h is the effective thickness of the hemisphere that is $2R/3$, For the methodology presented here, a control volume is defined to wrap around the hydrometeor. (b) Schematic illustrating the method for calculating the volume, area, and height of arbitrary geometry frozen hydrometeors on the hotplate.
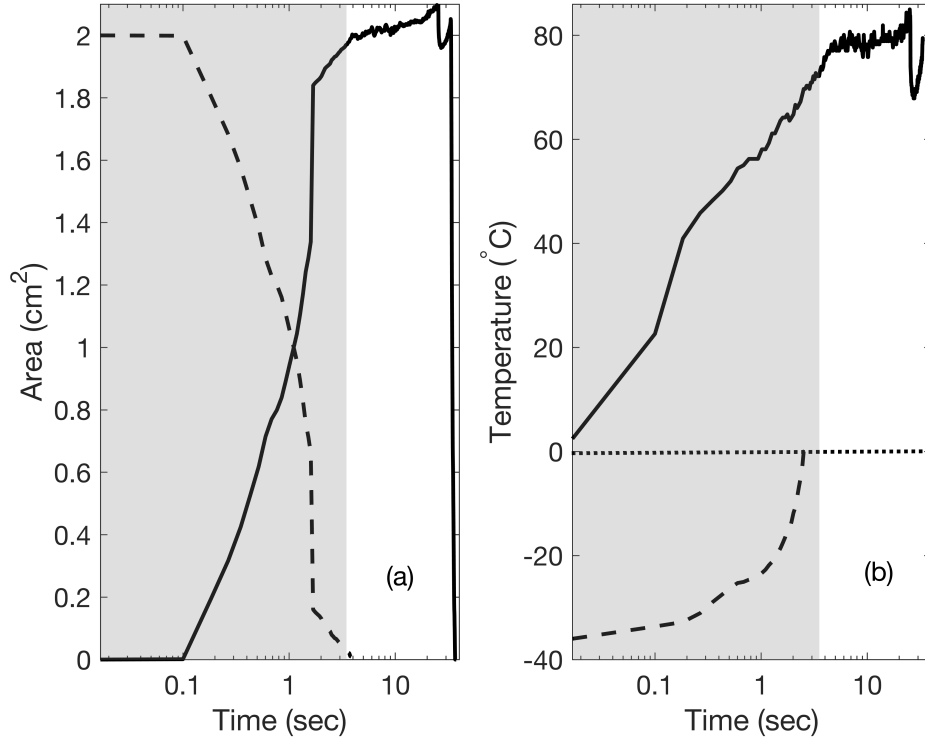
Figure 2. Observed melting and evaporation of a laboratory-made ice particle on the DEID hotplate. (a) Time series of the area of the ice particle (dashed black line) and the melted portion of the ice particle (solid black line). (b) The minimum surface temperature of the ice particle (dashed black line), and the temperature of the melted portion of the ice particle (solid black line) immediately after being placed on the hotplate. The horizontal dotted line represents a temperature partition in the melting and evaporation process. The shaded region denotes the period of melting. Details on the manufacture of the laboratory-made ice particles and experiments are provided in Section 3.1. The lag between melting and the evaporation start time is 0.1 s, which is equal to the thermal camera sampling period (sampling rate 10 Hz).

field experiments, the DEID measures Δt_{evap}, which is much longer than Δt_{melt}. Fortunately, a relation between Δt_{melt} and Δt_{evap} can be easily derived (see Appendix A). By estimating the average conductive heat-transfer rate during the melting and evaporation processes, we may substitute $\Delta T_{\text{melt}}\Delta t_{\text{melt}} \approx (L_{ff}/L_{vv})(\Delta T_{\text{evap}}\Delta t_{\text{evap}})$ into Eq. (6), which yields

$$\rho_{\text{MS}} = c\frac{m}{A_p\Delta T_{\text{evap}}\Delta t_{\text{evap}}}. \tag{7}$$

120   Here, the constant c is given by

$$c = (L_{ff})/(L_{vv}c_{\text{melt}}) \tag{8}$$

and has units of K s m^{-1}. The constant c is derived from a combination of thermodynamic and laboratory calibration constants that must be determined experimentally (see section 4.1).

In practice, Eq. (6) is evaluated following the methodology shown in Fig. 1b. Snowflakes of complex shapes do not have simple height relationships like $h = 2R/3$ as shown in Fig. 1a. Hence, a method is required to determine the height and volume of every pixel within a snowflake. If A_{ij} is taken as the area of ij^{th} pixel, h_{ij} the height of a frozen hydrometeor normal to the hotplate that is associated with the ij^{th} pixel, and $\mathcal{V}_{ij}$ is the volume of ij^{th} pixel, then we may write

$$\mathcal{V}_s = \sum_{ij} \mathcal{V}_{ij} = \sum_{ij} A_{ij} h_{ij} = c_{melt} \sum_{ij} A_{ij} \Delta T_{ij} \Delta t_{ij}, \tag{9}$$

which can then be estimated using the MS method on a pixel by pixel basis. Here, ΔT_{ij} is the temporal mean temperature difference across ij^{th} pixel, Δt_{ij} is the melting time of the ij^{th} pixel and c_{melt} is calibration constant of melting velocity. This study used Eq. (9) to calibrate laboratory ice particles and compare snowflake habits. For field observations, we make the following simplification to determine the volume

$$\mathcal{V}_s = c_{melt} A_p \frac{1}{n} \sum_{ij} \Delta T_{ij} \Delta t_{ij} \approx c_{melt} A_p \Delta t_{\mathrm{melt}} \frac{1}{n} \sum_{ij} \Delta T_{ij} = c_{melt} A_p \Delta T_{\mathrm{melt}} \Delta t_{\mathrm{melt}} = \frac{1}{c} A_p \Delta T_{\mathrm{evap}} \Delta t_{\mathrm{evap}} \tag{10}$$

Here, $A_p = n A_{ij}$ (assuming all pixels have the same area), n is the total number of a pixels associated with a frozen hydrometer, $\Delta T_{\mathrm{melt}} = \frac{1}{n} \sum_{ij} \Delta T_{ij}$ is the spatial and temporal mean temperature difference across a frozen hydrometer during melting, $\Delta t_{\mathrm{melt}} \approx \Delta t_{ij}$ is the melting time of a frozen hydrometer and $c = (L_{ff})/(L_{vv} c_{\mathrm{melt}})$.

Note that *are* impacted by variability in environmental conditions. A sample time series of temperature and hydrometeor area during melting and evaporation is shown in Fig. 2. During the melting process, the area of a particle that is in its frozen state decreases to zero from a maximum immediately after having fallen on the plate. At the same time, the observed liquid component of the hydrometeor increases to a maximum before abruptly disappearing. The sum of these two areas is nearly constant, at least accounting for inevitable uncertainties in the binary thresholding associated with discriminating the hydrometeor from its background. Notably, the sum is also equal to the initial area of the frozen particle prior to its melting. Figure 2 shows how the area of the ice particle prior to melting is similar to the maximum area of the liquid droplet showing that the area of solid hydrometeors is preserved after melting.

2.3 Use of the DEID to determine bulk snowpack-derived quantities

In additional to individual hydrometeor mass and density measurements, the DEID can be used to provide useful bulk snowpack quantities. Precipitation intensity or snow water equivalent rate of precipitation, $\dot{\mathrm{SWE}}$ (in mm hr^{-1}), can be estimated from the cumulative particle mass measured by the DEID over a given time period (Δt_{res}) as

$$\dot{\mathrm{SWE}} = k \frac{\Delta m}{\rho_w A_{hp} \Delta t_{\mathrm{res}}}, \tag{11}$$

where k is a conversion factor from m s^{-1} to mm h^{-1} (3.6×10^6 mm h^{-1} m^{-1} s), Δt_{res} is sampling time (h), Δm (kg) is the total hydrometeor mass that falls on the hotplate in given time, where individual mass of hydrometeor is estimated using Eq. (3), ρ_w (kg m^{-3}) is the bulk density of water and A_{hp} (m^2) is a rectangular sampling area on the hotplate that captures all hydrometeors. The accumulated SWE (mm) can be calculated over a given time interval Δt_{res} (h) as $\mathrm{SWE} = \dot{\mathrm{SWE}} \times \Delta t_{\mathrm{res}}$.

The average density ($\overline{\rho}_{\mathrm{MS}}$) of a freshly fallen snowpack layer can be estimated using the DEID from the ratio of the cumulative measured mass and the total volume of all snowflakes sampled in a given time interval (Δt_{res}) by assuming neither leaving any space between snowflakes nor overlapping,

$$\overline{\rho}_{\mathrm{MS}} = \frac{\sum_{i=1}^{N} m_i}{\sum_{i=1}^{N} m_i/\rho_{\mathrm{MS,i}}}, \tag{12}$$

where m_i (kg) is the mass of ith snowflake, $\rho_{\mathrm{MS,i}}$ (kg m^{-3}) the density of the ith snowflake, and N is the total number of snowflakes collected on the plate during the given time interval (Δt_{res}). From the average density of the snowflakes, the new snow accumulation rate $\dot{H}$ (mm h^{-1}) is then,

$$\dot{H} = k\frac{\Delta m}{\overline{\rho}_{\mathrm{MS}} A_{hp} \Delta t_{\mathrm{res}}}. \tag{13}$$

Finally, the total accumulated snow over H (mm) over a given time interval Δt_{res} (h) is given by $H = \dot{H} \times \Delta t_{\mathrm{res}}$. Note that the bulk density of a fresh snowpack and the height of snowpack can differ from the average density of individual snowflakes ($\overline{\rho}_{\mathrm{MS}}$) and H, respectively, because snowflake settling and compaction on the ground depend on considerations such as their settling characteristics, fall angle, wind speed, the structure of snowflakes, and ambient temperature. We do not account for these processes in the calculation of the volume of freshly fallen snow layers as the impacts are largely unknown. Hence, these variables are proxies for those in the actual snowpack.

3 Experimental Methods

Two laboratory experiments and one field experiment were designed to calibrate and validate the MS method for determining snowflake density. The first lab experiment was used to estimate v_{melt} of ice particles for a given set of environmental conditions and validate the density measurements of ice particles. The second lab experiment investigated the impact of environmental factors on v_{melt}. A field experiment was conducted at Alta Ski Area's mid-Collins snow-study plot to provide an opportunity to validate the MS method against manual measurements, ultrasonic snow-depth sensors, and a weighing gauge using an industry standard method.

3.1 Laboratory experiments method and validation

Laboratory experiments were conducted using: a DEID disdrometer, a 3D sonic anemometer (Campbell Scientific, Inc. CSAT3, sampling rate 20 Hz and accuracy $\pm$ 0.05 ms^{-1}), a temperature/relative-humidity sensor (Vaisala HMP 155, sample rate 1 Hz and accuracy $\pm$ 5% relative humidity, $\pm$ 1°C in temperature), a high-precision gravity scale (Sartorius model ENTRIS64-1S with a readability of 0.1 mg and a standard deviation of 0.1 mg), a micropipette (accuracy of 1% and maximum accuracy 1.2μL at highest volume), a silicon mold, and a freezer with a minimum temperature -37 °C. The precise setup of the DEID is modifiable, but for this study, the thermal camera measured surface temperatures of a hotplate with dimension $\approx$ 9 cm $\times$ 6 cm at 15 fps with 531 pixels $\times$ 362 pixels which yields a spatial resolution on the plate of about 0.2 mm/pixel. The thermal camera
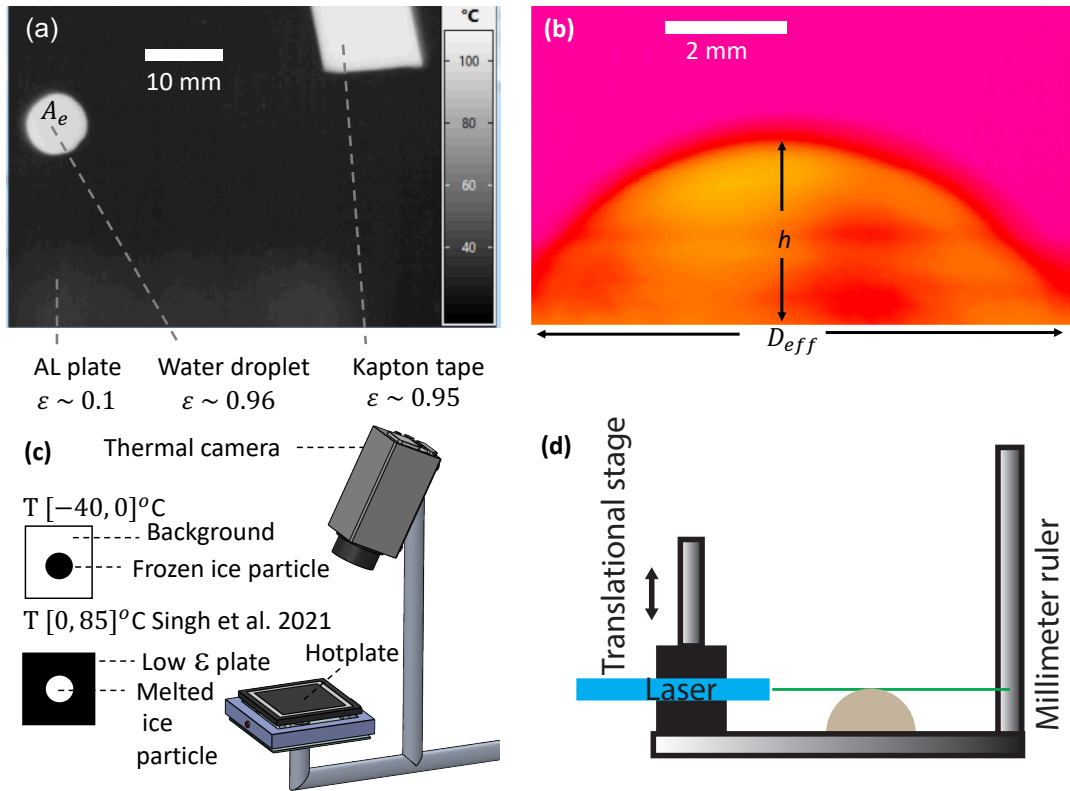
Figure 3. Details of the DEID MS measurement technique.(a) A hemispherical ice particle applied to the hotplate seen as a bright circular region after melting alongside a rectangular piece of Kapton tape ($\epsilon \approx 0.95$) used to measure hotplate surface temperature (T_p). (b) Side-view of a surface temperature contour plot of an ice particle obtained using the thermal camera at t = 0 and temperature range of thermal camera was used [-40,0]°C. (c) Schematic of the DEID showing the imaging of melting and evaporating particles, respectively. The black and white contrast of the ice and water particles is optimized by adjusting the camera's temperature range. (d) Schematic of the ice-particle height measurement apparatus.

was looking vertically downward at the hotplate at an angle. As a result, the maximum error in area measurement is 1.6%, and the error in the area was corrected using a custom-made function based on the height and angle of the thermal camera, and details are given in Appendix D. Continuous thermal-camera imagery (recorded at 15 Hz) provided all relevant parameters for calculating hydrometeor mass, except for the effective thermal-conduction coefficient between the hotplate and hydrometeor (κ), which was determined through laboratory calibration. We used an Infratec thermal camera that writes out infrared binary (IRB) files that store each pixel's absolute temperature. In post-processing, a gray-scale thermal image ranging in intensity from 0 to 255 is created from the IRB files based on a preset infrared temperature range. For determining Δt_{melt} and ΔT_{melt}, the temperature range used was [– 40, 0] °C, and for the m, A_p, Δt_{evap}, and ΔT_{evap} measurements, the temperature range used was [0, 85] °C. In a table-top experiment, the DEID was operated at 85 °C as determined using the thermal camera. To measure v_{melt} using h and Δt_{melt}, the DEID was placed in a 0.25 m per side open-topped cubic enclosure with in an environment with

a near-zero wind-tunnel wind speed of 0.02 m s^{-1}, a constant ambient temperature of 18 °C, and a constant relative humidity of 38%. Eighty hemispherically-shaped ice particles with a range of known masses and volumes were made in a laboratory

195 freezer using a micropipettor by applying a distilled water droplet to a flat silicon mold. Droplet volumes of 5, 10, 20, 30, 40, 50, 60, and 70 μL, with ten samples per volume, were used to manufacture the ice particles. The height of the ice particles h

Table 1. The shape of sample ice particles made in a laboratory: $\mathcal{V}_{\mathrm{pipette}}$ is the volume of water applied by the pipette, A_p is the cross-sectional area of ice particles measured by the thermal camera on the hotplate, and h is the maximum thickness of ice particles determined from the laser pointer system.

$\mathcal{V}_{\mathrm{pipette}}$ (μL)	A_p (mm^2)	h (mm)
5	5.65 $\pm$ 0.09	1.21$\pm$0.07
10	9.10 $\pm$ 0.09	1.64$\pm$0.03
20	13.90 $\pm$ 0.11	2.23$\pm$0.08
30	17.60 $\pm$ 0.09	2.54$\pm$0.03
40	22.61 $\pm$ 0.11	2.28$\pm$0.07
50	26.81 $\pm$ 0.17	2.85$\pm$0.05
60	31.13 $\pm$ 0.16	3.25$\pm$0.09
70	34.56 $\pm$ 0.14	3.34$\pm$0.08

was measured in the freezer as illustrated in Fig. 3d. A U-shaped rigid metallic frame was mounted on a translational stage. A millimeter ruler was attached to one arm of the U-frame, and a laser pointer was affixed perpendicularly to the second arm facing towards the ruler on the opposite arm in such a manner that when turned on, the pointer's laser beam would strike a spot

200 on the ruler bar. The pointer was horizontally aligned independently using a precision bubble level. The ice particle was thus positioned between the two arms of the U-frame. The ruler scale's purpose was to obtain the vertical height of the ice particles. The U-frame was vertically displaced when the ice particle occluded the laser beam and did not reach the ruler scale. Upon emerging at the top of the ice particle, when the beam spot hit the ruler scale, the reading was taken as illustrated in Fig. 3d. Furthermore, ice particle mass was also measured with a gravimetric scale prior to its application on the hotplate.

205 Individual frozen droplets were placed on the hotplate, and the cross-sectional area A_p, m, ΔT_{melt}, ΔT_{evap}, Δt_{melt} and Δt_{evap} were measured using the DEID from Eq. (3). v_{melt} was then calculated using two different formulas $v_{\mathrm{melt}} = h/\Delta t_{\mathrm{melt}}$ and using Eq. (5), where h determined from the laser pointer system.

3.2 Environmental impacts on v_{melt} measurement: wind-tunnel experiments

For any given ice-particle mass m, independent of the rate of melting or evaporation, the $\approx m(L_f + L_v)$ constant total quantity

210 of energy is required both to melt and to evaporate a particle from the hotplate. However, the conductive heat rate from the hotplate to the ice particle is a function of environmental conditions through the temperature difference ΔT. To determine how environmental variability affects measurement of the melting velocity v_{melt}, a portable wind tunnel was set on one side of the DEID's hotplate, allowing different wind velocities to pass over the hotplate and ice particles. A pitot-static probe and
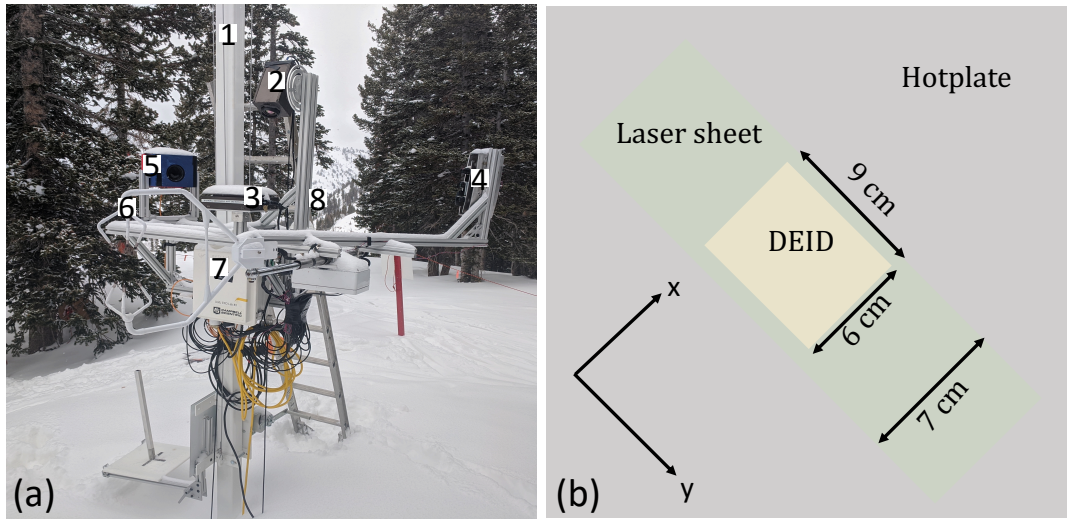
Figure 4. (a) Field experimental set-up for measurements of microphysical properties of snowflakes and snowflakes visualization. The experimental set-up consists of (1) 20 – m tower (2) a thermal camera (3) Hotplate (4) Three 10-W lasers and optical lens (5) D850 Nikon SLR camera (6) 3-D sonic anemometer (7) data logger/computer and (8) relative humidity and temperature sensor. (b) Top-view schematic showing the co-location of the laser system and DEID hotplate.

an automated weather station measured air speed, ambient temperature and relative humidity. 60-μL (0.06 g) ice particles with thickness $h = 3.25$ mm and area $A_p = 30.13 \times 10^{-6}$ m^2 were placed on the DEID's hotplate. Three experiments were performed. First, the hotplate temperature and the ambient relative humidity were maintained constant at 85°C and 38%, respectively, while the wind tunnel was adjusted for air speeds of 0.0, 1.5, 3.0, 4.7, 5.9, and 8.3 m s^{-1}. Second, ice particle experiments were performed for surface plate temperatures of 65 °C, 85 °C, and 95 °C for near-zero wind speed and 38% relative humidity. Finally, the relative humidity was varied to cover 38%, 68%, and 91% with near-zero wind speed and constant hotplate temperature 85°C.

3.3 Density of individual frozen salt-water particles

To test the MS method on a wide range of particle densities, a method was required to produce particles of varying densities. This was done by creating frozen droplets by adding sodium chloride in a distilled water solution, and the percentage of sodium chloride is provided in Table 4. The densities of these particles were then measured using the DEID and the same methods described above for the pure frozen-water tests.

3.4 Field validation experiments

Data were obtained from field experiments conducted during the winter between October 2020 and April 2021 comprising seventeen snowfall events in Upper Little Cottonwood Canyon, Utah, USA at the Alta Ski Area's mid-Collins snow-study Plot

(Alcott and Steenburgh, 2010) (40.5763 °N, 111.6383 °W, 2920 m above sea level). A 10-m crank-up measurement tower at the site included a DEID (sampling rate 15 Hz) for measurement of microphysical properties of snowflakes. In addition to the DEID, a particle imaging system was simultaneously deployed that consisted of a laser sheet with a sampling volume of 10 cm × 18 cm × 7 cm that was oriented normal to the viewing angle of a Nikon D850 single-lens reflex (SLR) camera as shown in Fig. 4a. The SLR camera recorded 1920 pixel × 1080 pixel images at a spatial resolution ≈ 160 μm/pixel at 120 fps within a vertical laser sheet created using three 10-W, 520-nm diode lasers and a collimator lens. The laser beam spread angle of ≈ 6.8° allowed for a light sheet with near constant thickness of ≈7 cm throughout the region of interest. A single focal length Nikon AF-S VR Micro-Nikkor 105 mm f/2.8 G IF-ED lens permitted a depth-of-field greater than the thickness of the laser light sheet. The DEID was deployed 2 cm below the lower end of laser sheet, which permits measurement of the microphysical properties of snowflakes that pass the laser sheet and fall on the hotplate. A Vaisala HMP 155 temperature and relative humidity sensor (1 Hz sampling rate) was also located on the tower and maintained at a height of approximately 1.5 m above the new snow level. At approximately the same height, a Campbell Scientific, Inc. CSAT3 3D sonic anemometer was deployed (sampling rate 20 Hz).

Images from the SLR camera were combined with mass measurements from the DEID to compute snowflake density in the field and validate the MS method. With this SLR-DEID method, the geometrical volume of each free falling snowflake was estimated using images from the SLR camera. The mass of each hydrometeor was determined by following individual snowflakes through the laser sheet until they hit the DEID hotplate. This method was applied to approximately 1000 snowflakes. Selected thermal images of aggregate snowflakes and graupel on the hotplate are illustrated in Appendix B.

3.5 Hydrometeor density calculation exploiting concurrent imagery during their fall

The geometrical volume $\mathcal{V}_{\mathrm{SLR}}$ of a snowflake can be estimated independently from the DEID by imaging falling snowflakes using the particle tracking system discussed above. In this case, the density is determined from

$$\rho_{\mathrm{SLR\text{-}DEID}} = \frac{m}{\mathcal{V}_{\mathrm{SLR}}}, \tag{14}$$

where snowflake mass m is determined with the DEID from Eq. (3).

We categorized five snowflake habits based on the international classification for seasonal snow on the ground (Fierz et al., 2009; Praz et al., 2017), planar crystal (combining stellar and plates), graupel (combining hail and graupel), columnar crystal, aggregate (combining irregular crystal), and small particles. Graupel and small particle crystals were classified based on size. Each snowflake category contained approximately 200 samples. Taking advantage of how snowflakes rotate while falling, a single camera with multiple images was found to represent a three-dimensional picture of a snowflake and provide geometrical volume more accurately than using a single image (Li et al., 2022). Five sequential selected images of each crystal type are illustrated in Fig. 5a. A schematic showing how snowflake volume is computed is illustrated in Fig. 5b and formulated in Table 2 . The volume of planar crystals was approximated as a disc, hence, $\mathcal{V}_{\mathrm{SLR}} = A_{\max} D_{\min}$. Here, $A_{\max}$ is the maximum area of a planar crystal in a 2-D plane among all the images that are visible by the camera and $D_{\min}$ is the minimum dimension (representing the thickness of the disc) in the 2-D plane as indicated in Fig. 5a column I row V. The volume of graupel was es-
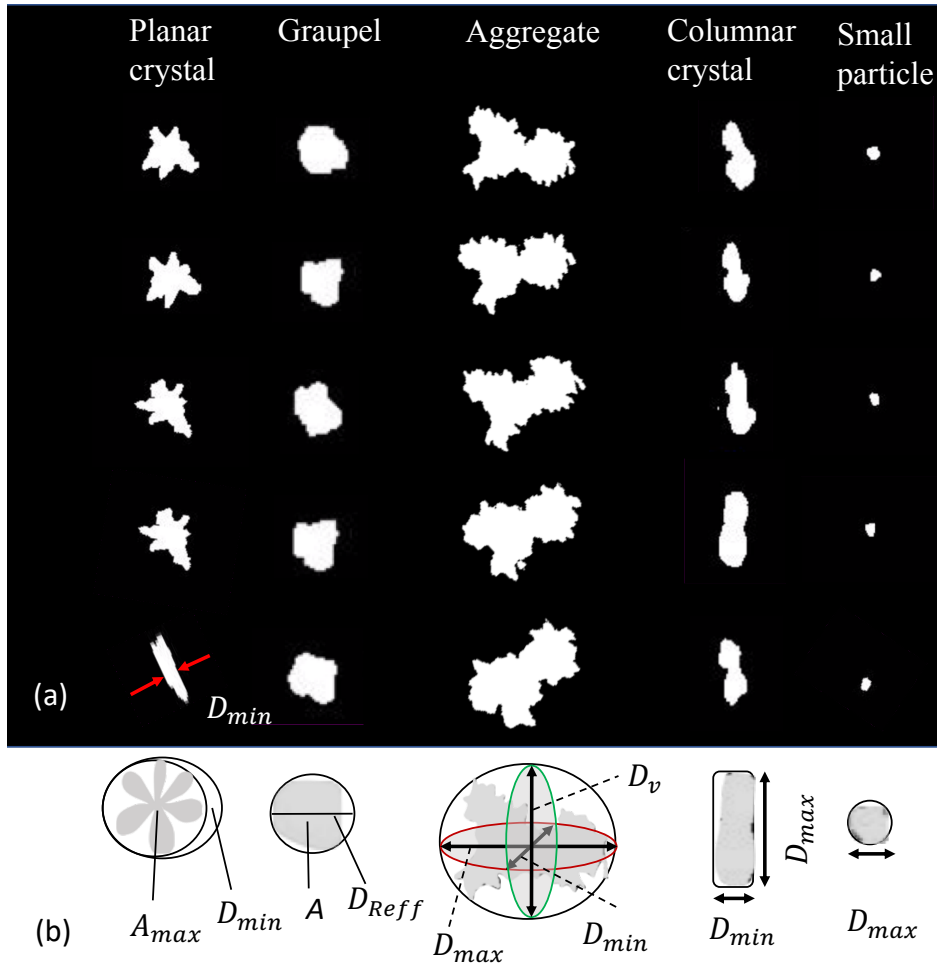
Figure 5. (a) For five snowflake types, five images of each snowflake separated due to rotation just prior to settling on the DEID's hotplate. (b) Volume measurement method

timated as a sphere $\mathcal{V}_{\mathrm{SLR}} = \pi/6D_{\mathrm{Reff}}^3$, where D_{Reff} is the effective circular diameter estimated using the SLR camera imaging the snowflake falling in the air and estimated as a $D_{\mathrm{Reff}} = \sqrt{\frac{4}{\pi}\overline{A}}$. $\overline{A}$ is the two-dimensional mean area of all images as illustrated in Fig. 5a column II. The volume of aggregates was estimated by fitting an ellipsoid such that $\mathcal{V}_{\mathrm{SLR}} = \frac{\pi}{6}D_{\mathrm{max}}D_{\mathrm{min}}D_v$, where D_{max}, D_{min} and D_v are illustrated in Fig. 5b. The volume of columnar crystals (solid cylinder) was estimated from $\mathcal{V}_{\mathrm{SLR}} = \frac{\pi}{4}\overline{D}_{\mathrm{min}}^2\overline{D}_{\mathrm{max}}$, where $\overline{D}_{\mathrm{max}}$ and $\overline{D}_{\mathrm{min}}$ are the average of the maximum and minimum dimensions of five images as illustrated in Fig. 5a, column III . The volume of small particles were estimated using a spherical volume $\mathcal{V}_{\mathrm{SLR}} = \frac{\pi}{6}\overline{D}_{\mathrm{max}}^3$, where $\overline{D}_{\mathrm{max}}$ is the average of the maximum dimension of five small particle images (Fig. 5a column V).

Table 2. Classification of snowflakes and corresponding volume estimation based on crystal geometry.

Snow crystal type	Geometrical shape	Volume ($\mathcal{V}_{\mathrm{SLR}}$)
Planar	Disc	$A_{\max} D_{\min}$
Columnar	Solid cylinder	$(\pi/4)\overline{D}_{\min}^2 \overline{D}_{\max}$
Graupel	Spherical	$(\pi/6)D_{\mathrm{eff}}^3$
Small particle	Spherical	$(\pi/6)\overline{D}_{\max}^3$
Aggregate	Ellipsoid	$(\pi/6)D_{\max}D_{\min}D_v$

3.6 Manual measurements of the snowpack: Bulk-density snowpack calculations

270 The mean bulk density of a fresh snowpack(ρ_s^m) can also be determined using manual measurements of the ratio of the snow water equivalent depth (SWE) to the new snow depth (H). This can be done with the DEID by recalling that $\mathrm{SWE} = k\Delta m/\rho_w A_{hp}$ and $H = k\Delta m/\rho_s^m A_{hp}$,

$$\rho_s^m = \rho_w \frac{\mathrm{SWE}}{H}. \tag{15}$$

where ρ_w is the density of water of $1000\,\mathrm{kg\,m^{-3}}$. At the Alta-Collins snow-study plot these measurements were obtained every 275 12 hours. Note that changes within the snowpack due to such processes as densification, heat transfer, wind shear, etc., are not considered here as analyses are limited to consideration of freshly fallen snow.

For further comparison, the average snowpack density can also be estimated at hourly intervals based on measurements obtained from an ETI Instrument Systems Noah-II precipitation weighing gauge ($\mathrm{SWE}_{\mathrm{ETI}}$) and the snow depth from a Campbell Scientific, Inc. SR50 ultrasonic snow-depth sensors. The ETI and SR50 sensors were deployed 4 m from the DEID at the 280 Alta-Collins site. A windshield was deployed around the ETI bucket to increase catchment efficiency. The ETI reported SWE measurements once every hour with a resolution, threshold, and accuracy of 0.25 mm, 0.25 mm, and $\pm$ 0.25 mm respectively. The SR50 sensor recorded snow depth every hour to provide running totals of snow depth. The measurement range of the ultra-sonic sensor was 0.5 m to 10 m with an accuracy of 0.4% and a resolution of 0.1 mm. Raw DEID data sampled at a rate of 15 Hz were integrated to produce hourly measurements for comparison with ETI data. ETI and SR50 data were collected 285 throughout the winter of 2020, but data from 0700 UTC 12 Dec to 1900 UTC 12 Dec 2020 were used to compare SWE and snow accumulation with the DEID obtained using the MS density measurement method.

4 Results

4.1 MS density method laboratory calibration

In order to use the MS method for determining density, the melting calibration constant c_{melt} and the calibration constant c 290 in Eqs. (5) and (7), respectively, must first be determined empirically. To do this, eighty ice particles with different sizes and

masses were applied to the DEID hotplate. Furthermore, the experiments were conducted in an environmentally controlled chamber with the air temperature fixed at 18 °C, near-zero wind velocity (0.05 m s^{-1}), a hotplate temperature of 85°C, and 38% relative humidity. Results from experiments conducted at these standard conditions are identified with a subscript 0. The variables Δt_{melt}, Δt_{evap}, ΔT_{melt}, and ΔT_{evap} for each particle were determined using the thermal camera, while h was measured directly using the laser-pointer system. The measured values of h and Δt_{melt} are plotted in Fig. 6a. The slope of the h-Δt_{melt} curve is v_{melt}, which is approximately constant ($v_{0,\mathrm{melt}} = 2.11 \pm 0.10 \times 10^{-4}$ m s^{-1}) because the experiments were performed with ice-particles in an environmentally controlled chamber where the average measured value of $\Delta T_{0,\mathrm{melt}}$ was also found to be approximately constant (101.43 ± 0.82 K).

The measured v_{melt} and ΔT_{melt} for each particle can be substituted into Eq. (5) to solve for c_{melt}, and then the constant c can easily be determined from Eq. (8). This was done and the results were averaged over all 80 samples, yielding $c_{\mathrm{melt}} = 2.08 \pm 0.11 \times 10^{-6}$ m$^{-1}K^{-1}$ and $c = 7.14 \pm 0.33 \times 10^{4}$. With a derived value of c and particle mass measured with the DEID, the particle density can now be inferred from Eq. (7). This yields an average ice-particle density of $\rho_{\mathrm{MS}}^{\mathrm{ice}} = 919 \pm 65$ kg m^{-3}. This is very close to the expected value of ice density at temperatures near 0°C (i.e., 917 kg m^{-3}).

A summary of the following measured parameters for laboratory-created ice particles are presented in Table 3: v_{melt}, $\rho_{\mathrm{MS}}^{\mathrm{ice}}$, m_{DEID}, m_{gravity} and $\mathcal{V}_{\mathrm{pipette}}$. Here, $\mathcal{V}_{\mathrm{pipette}}$ is the volume of a water droplet, not the ice particle volume. Since these experiments were conducted in an enclosure where environmental variability was negligible and the effect of convective cooling on the measurement of m, A_p, Δt_{melt} Δt_{evap}, and ΔT_{evap} did not play a role. However, in nature, winds can affect Δt_{melt} Δt_{evap}, and ΔT_{evap} as well as v_{melt}.

Table 3. Mean and standard deviation of the mass of eighty experimentally manufactured ice particles the water droplet volume applied by pipette ($\mathcal{V}_{\mathrm{pipette}}$) prior to freezing, determined using a gravimetric scale (m_{gravity}) and the DEID (m_{DEID}). The density of ice particles estimated using the DEID MS method (ρ_{MS}^{ice}), and the melting velocity $v_{0,\mathrm{melt}}$ (ms^{-1}) under the standard conditions described in the text.

$\mathcal{V}_{\mathrm{pipette}}$ (μL)	m_{gravity} (mg)	m_{DEID} (mg)	ρ_{MS}^{ice} (kg m^{-3})	$v_{0,\mathrm{melt}} \times 10^{-4}$ (m s^{-1})
05	5.6 ± 0.4	5.1 ± 0.2	926 ± 32	2.15 ± 0.14
10	12.3 ± 0.7	14.0 ± 0.8	916 ± 58	2.09 ± 0.12
20	21.6 ± 0.8	22.1 ± 1.0	942 ± 61	2.11 ± 0.12
30	30.8 ± 2.7	29.8 ± 2.0	938 ± 84	2.16 ± 0.16
40	42.0 ± 3.2	43.1 ± 3.4	906 ± 58	2.04 ± 0.09
50	53.1 ± 4.1	52.1 ± 2.4	901 ± 67	2.08 ± 0.11
60	61.8 ± 3.8	63.1 ± 3.8	928 ± 76	2.12 ± 0.07
70	74.1 ± 4.1	76.2 ± 4.2	899 ± 86	2.14 ± 0.04
			919 ± 65	2.11 ± 0.10

To determine how environmental variability affects v_{melt} and to generalize the validation of Eq. (5), 60-μL (0.06 g) ice particles with thickness $h = 3.25$ mm and area $A_p = 30.13 \times 10^{-6}$ m^2 were placed on the DEID's hotplate and the wind speed was varied from 0.0 to 8.3 m s^{-1}, relative humidity varied from 38% to 91%, and plate temperature varied from 65°C to
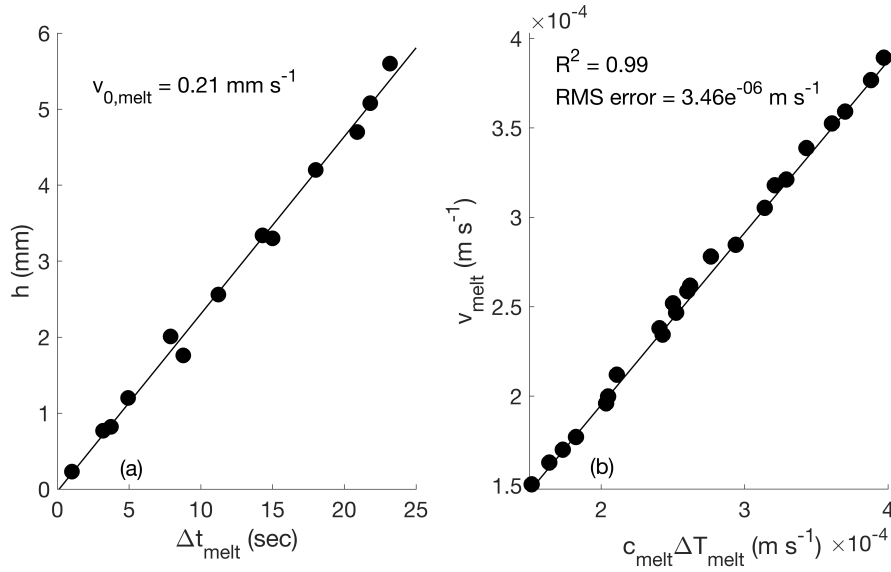
Figure 6. (a) Ice-particle height as a function of Δt_{melt}, the slope of this line determines $v_{0,\text{melt}}$, the melting speed under fixed standard conditions. That is, ice particles of different maximum thickness [0.22, 5.6] mm and their melting time at a plate temperature of 85°C, near-zero wind velocity (0.05 m s^{-1}), and 38% relative humidity. (b) Plot of v_{melt} versus $c_{\text{melt}}\Delta T_{\text{melt}}$ illustrating the validity of Eq. (5). v_{melt} is determined directly from measurements of particle maximum thickness, h and melting time, Δt_{melt} and then compared to $c_{\text{melt}}\Delta T_{\text{melt}}$ for a range of environmental conditions.

95°C. v_{melt} was computed using direct measurements and computed as $v = h/\Delta t_{\text{melt}}$. It was also computed using Eq. (5, i.e., $v_{\text{melt}} = c_{\text{melt}}\Delta T_{\text{melt}}$. Results are shown in Fig. 6b. The coefficient of determination R^2 between v_{melt} computed using the two methods is 0.99, and the RMS error is 3.46×10^{-6} m s^{-1}. Using Eq. (7), the average measured density of 80 ice particles with

315   different shapes and sizes and was made by pipetting water droplets onto arbitrary surfaces with different contact angles, with the above listed environmental conditions and plate temperatures, was 928 ± 56 kg m^{-3}, which shows the MS method works for a wide range of environmental conditions to within experimental uncertainty.

4.2   Density of individual frozen salt-water particles

To test the MS method on a wider range of particle densities, frozen salt-water particles with different salt (NaCl) concen-

320   trations were applied to the DEID hotplate. The estimated density of the frozen salt-water particles calculated using the MS method agrees with the density expected from the percentage of salt in the solution ($\rho_{\text{theoretical}}$) to within 3%. The results are summarized in Table 4.

Table 4. The density of frozen salt-water particles measured using the MS method and determined theoretically based on a salt-water ratio by weight (percentage of salt and water).

Percentage of salt (%)	Percentage of water(%)	ρ_{MS} (kg m^{-3})	$\rho_{\mathrm{theoretical}}$ (kg m^{-3})
1.47	98.52	969 ± 37	1008
2.75	97.24	988 ± 26	1015
5.07	94.92	1002 ± 38	1028
7.16	92.83	1018 ± 24	1040
8.86	91.13	1028 ± 31	1050
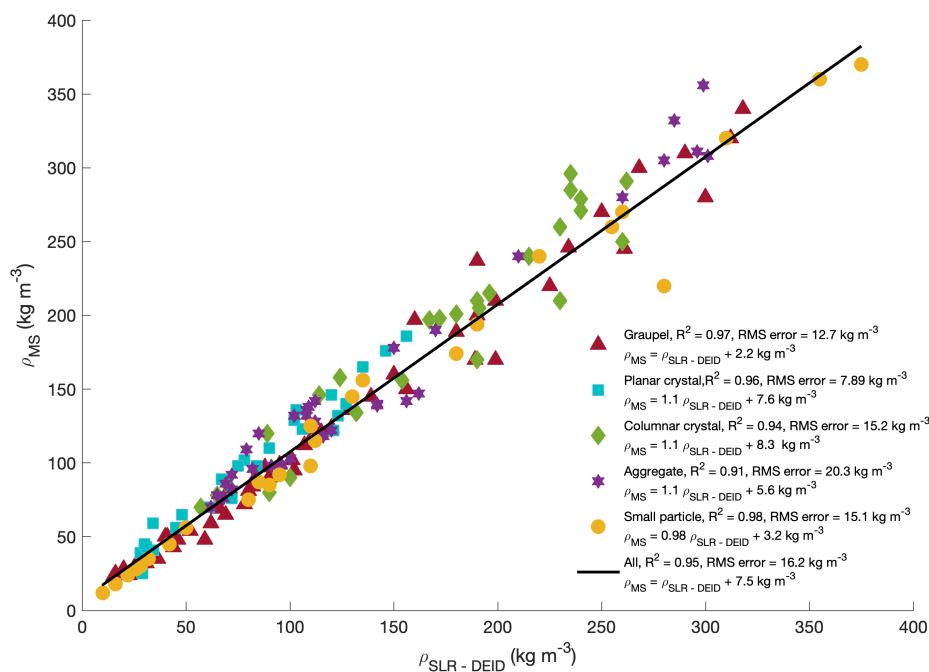
Figure 7. Measured density of a range of snowflake types using the particle imaging system compared with values obtained using the DEID MS method with associated coefficients of determination, slopes and RMS errors.

4.3 Field evaluation of the MS method for snow particles of different types

We collected data at Alta Ski Area's mid-Collins snow-study plot from 07 November 2020 to 27 April 2021. During this time, a snow accumulation of 12.35 m and a SWE accumulation of 1.38 m were observed with the DEID. The ambient air temperature varied from –21°C to 2°C, relative humidity varied from 64 to 97%, and wind speed varied from 0.2 to 8 m s^{-1}. Generally, the observed densities of freshly fallen individual snowflakes varied from 9 to 495 kg m^{-3}. The average densities of each storm

Table 5. Camparision between two density methods, MS and SLR-DEID of five types of snow crystal. Range of D_{eff} for each type of crystal.

Snow crystal type	D_{eff} (mm)	ρ_{MS} (kg m^{-3})	$\rho_{\text{SLR-DEID}}$ (kg m^{-3})	Uncertainty (%)	R^2
Planar	2.4 - 4.3	89 $\pm$ 40	98 $\pm$ 46	9.6	0.96
Columnar	1.4 - 3.4	157 $\pm$ 82	140 $\pm$ 92	11.4	0.95
Graupel	1.4 - 4.6	120 $\pm$ 87	130 $\pm$ 89	3.7	0.97
Small particle	0.8 - 1.2	141 $\pm$ 109	138 $\pm$ 110	2.1	0.98
Aggregate	3.1 - 10.2	188 $\pm$ 72	170 $\pm$ 64	10.1	0.91

varied from 35 to 115 kg m^{-3}. Figure 7 shows estimated snowflake densities using both the SLR-DEID and MS methods for five types of snowflakes. A comparison between the MS and SLR-DEID density methods for five crystal types is summarized in Table 5. The coefficient of determination between the two methods is highest for small particles and graupel and least for aggregates. The measured size (D_{eff}) of each type of crystal is summarized in Table 5. The uncertainty that arises between the two methods for aggregate snowflakes may be due to the SLR-DEID's method used to estimate the geometrical volume because aggregate have have a more irregular shape than the other types. For all snowflakes, the mean estimated density is 131 $\pm$ 83 using the SLR-DEID method and 142 $\pm$ 87 using the MS method, yielding an uncertainty of 3.9% and an R^2 of 0.95.

4.4 Frequency distribution of individual hydrometeor densities

Figure 8a shows a probability distribution function (PDF) for the densities of individual snowflakes using the MS method applied to data acquired at the Alta-Collins snow-study plot for seven snow storms selected to encompass a broad range of environmental conditions: mean ambient temperatures [-13.45, -4.82] $^\circ$C, mean wind speeds [0.30, 0.89] ms^{-1}, and mean relative humidities [72, 91]% as listed in Table 6. The kurtosis (Kr) and skewness (Sk) of the normalized density distribution functions vary from 2.02 to 2.42 and 0.01 to 0.10, respectively. We found that the PDFs of snow density are symmetric about the mean ($Sk = 0.01$) and near Gaussian ($Kr = 2.41$) when the ambient temperature is lowest, while $Sk = 0.10$ and $Kr = 2.02$ when the ambient temperature is highest, which is shown in Table 6. Figure 8b includes results from snowflake densities computed assuming a spherical particle volume but also using the DEID, as done in (Rees et al., 2021). The spherical assumption underestimates snowflake density by a factor ≈ 1.5 compared to the MS method.

4.5 Validation of SWE measurements

SWE determined with the DEID can be compared to manual measurements collected at the Alta-Collins study plot. Since manual measurements are made infrequently at intervals of 12 hours, the comparisons are made on a storm-by-storm basis as shown in Fig. 9. The relationship between DEID observations and the bulk standard manual measurement techniques is shown in Fig. 9a. A best fit relationship between the two methods yields an R^2 of 0.994 with a slope of 0.94 $\pm$ 0.04.
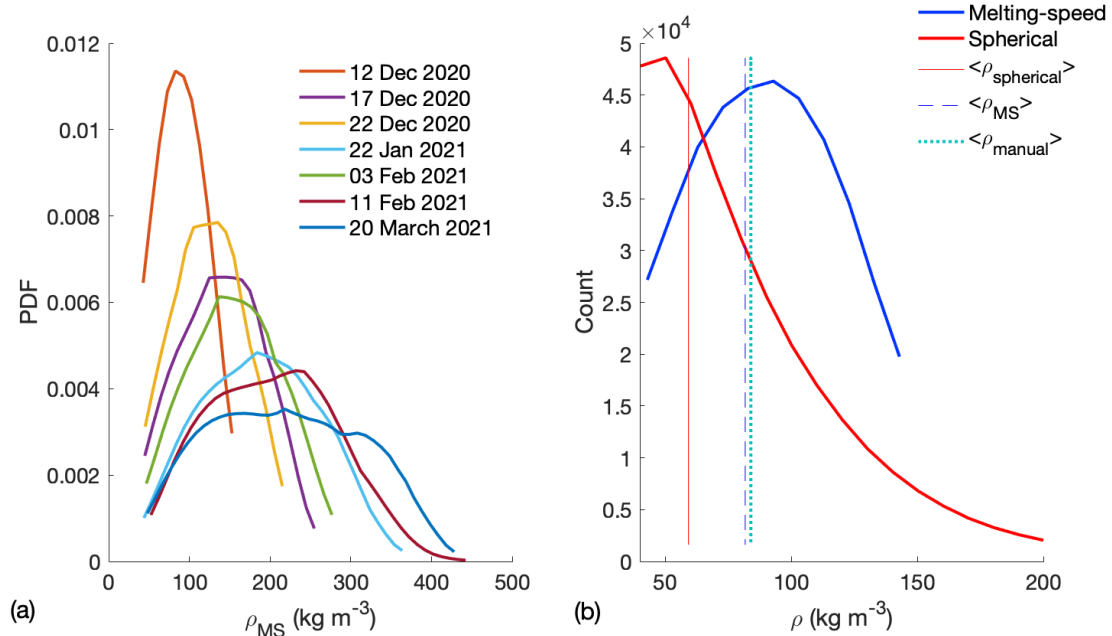
Figure 8. (a) Probability distribution functions of density of individual snowflakes measured using the MS method for seven storms. (b) Comparison between density determined with two methods employing DEID measurements alone, the MS method and the spherical particle method. The solid line, dash line, and dot line are the mean density of a storm using a spherical method, MS method and manual measurements, respectively. Note that the MS method and manual measurement are compared without knowing the information about snowpack, as we mentioned earlier.

350   The accumulated SWE integrated over one-minute intervals is compared to ETI data in Fig. 9b. DEID SWE accumulation observations match those from the ETI gauge to within ± 6% over the 12-hour measurement period (storm duration). SWE accumulation measured by the DEID is slightly higher than that obtained by the ETI because the minimum resolution of the ETI is 0.254 mm, whereas the minimum DEID resolution is 0.001 mm (Singh et al., 2021). Furthermore, the ETI gauge has been shown to undercatch snowflakes compared to the DEID under high-wind conditions (Singh et al., 2021).

355 **4.6   Validation of Snow depth measurements**

Snow accumulation (H) was computed with the DEID using Eq. (13) and $H = \dot{H} \times \Delta t_{\text{res}}$, where 1-min average MS density was used. The total snow accumulated in each storm measured using the DEID MS density method compares well with manual measurements obtained every 12 hours at the Alta-Collins snow-study plot with an R^2 value of 0.983 and a slope of 1.12 ± 0.07 as shown in Fig. 10a. A 12-hour period with snowfall between 0700 UTC and 1900 UTC 12 Dec 2020 is shown in Fig.
360 10b. There is also good agreement to within ± 5% between snow accumulation measurements obtained from the DEID using the MS-density method and those obtained using an ultrasonic snow-depth sensor obtained once per hour. The bulk density of a fresh snowpack can differ from the average density of individual snowflakes and the 1-min average because snowflake settling
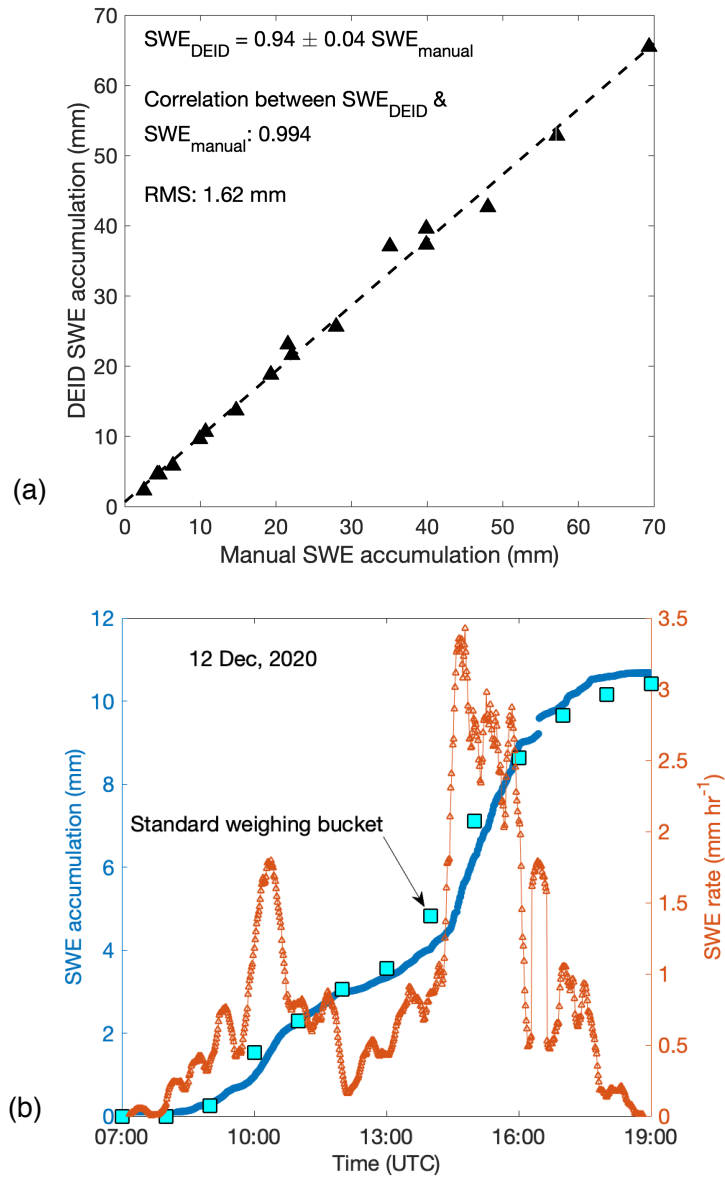
Figure 9. (a) SWE accumulation from DEID and manual measurements for seventeen storms. Each data point represents an individual storm. Manual measurements were made every 12 hours (1100 UTC and 2300 UTC), and the DEID sampled at 15 Hz. (b) Time series of SWE accumulation and SWE rate measured using the DEID and ETI gauge. Each DEID data point represents a 1-min average and each ETI-gauge data point a 1-hour average.
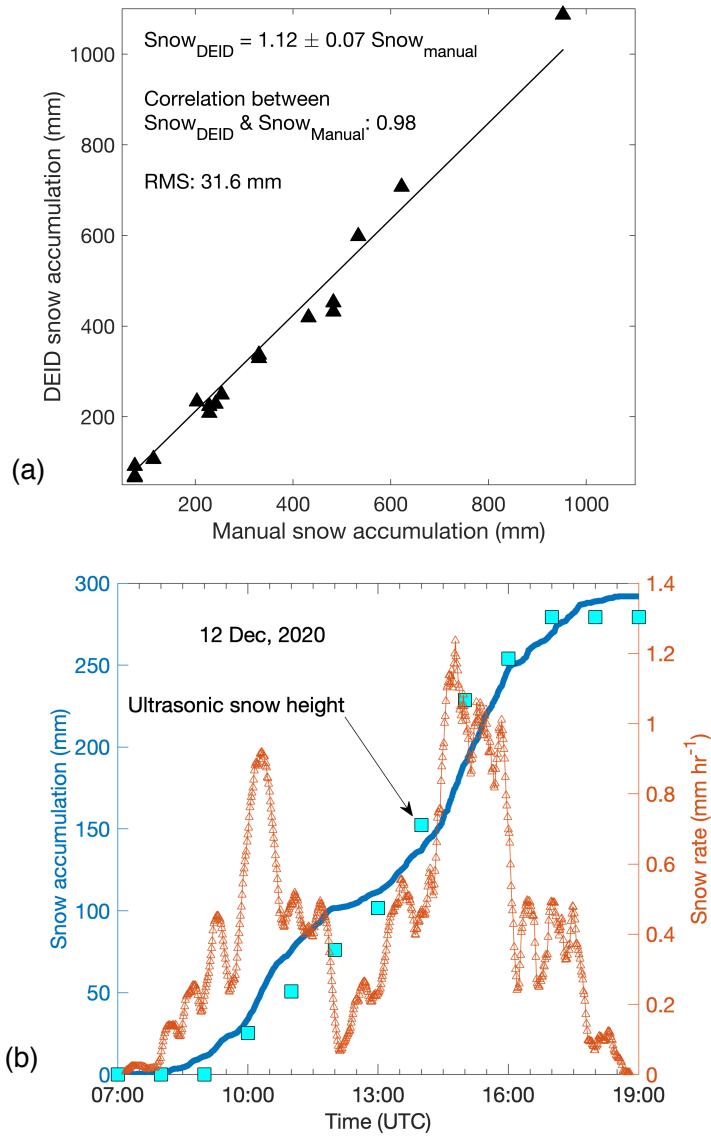
Figure 10. (a) For seventeen storms, comparison between snow accumulation from the DEID obtained using the MS density method and from manual measurements made every 12 hours (1100 UTC and 2300 UTC). Each data point represents a storm. (b) Time series of snow accumulation and snowfall rate measured using 1-min averaged DEID results and 1-hour averaged ultrasonic snow-depth sensor measurements during a storm on 12 December 2020.

Storm Day/duration (Hours)	N	$\overline{D}_{\mathrm{eff}}$ (mm)	$\overline{\rho}_{\mathrm{MS}}$ (kg m^{-3})	$\overline{T}_{\mathrm{amb}}$ (°C)	$\overline{U}$ (m s^{-1})	$\overline{RH}$ (%)	total Snow (mm)	total SWE (mm)	Kr	Sk
Dec 12 2020/20	242,643	1.60 ±0.74	41.86	-13.45 ± 1.37	0.58	85.24	292	10.66	2.42	0.01
Dec 17 2020/25	482,152	1.50 ±0.71	56.25	-6.75 ± 2.30	0.30	90.86	413	27.00	2.18	-0.07
Dec 22 2020/24	251,532	1.50 ±0.71	49.19	-12.08 ± 4.72	0.76	81.15	314	15.38	2.39	0.03
Jan 22 2021/45	570,590	1.50 ±0.68	90.54	-6.82 ± 2.29	0.65	90.28	457	34.37	2.14	0.05
Feb 03 2021/62	653,976	1.40 ±0.65	65.30	-9.98 ± 2.54	0.76	89.55	488	31.75	2.27	0.02
Feb 11 2021/67	1,275,102	1.50 ±0.59	56.27	-7.29 ± 3.17	0.56	86.56	862	51.81	2.16	0.03
March 20 2021/24	629,870	1.60 ±0.78	88.76	-4.82 ± 3.07	0.89	71.71	425	35.35	2.02	0.10

Table 6. Summary of DEID-derived snowflake parameters for a series of storms in Alta, Utah. Mean diameter $\overline{D}_{\mathrm{eff}}$, mean density $\overline{\rho}_{\mathrm{MS}}$, and total number of snowflakes N captured during seven storms with a mean ambient temperature $\overline{T}_{\mathrm{amb}}$, mean wind speed $\overline{U}$, mean relative humidity $\overline{RH}$, total snow and total accumulated snow water equivalent for seven storms using the DEID. Kr is the Kurtosis and Sk the Skewness of the density distribution.

and compaction on the ground depends on such considerations as their settling characteristics, fall angle, wind speed, the structure of snowflakes, and the ambient temperature. We do not account for these processes in the calculation of the volume of
365   freshly fallen snow layers as the impacts are largely unknown. Nonetheless, The bulk density of the snowpack measured during seventeen storms using the DEID MS method, can also be compared with manual gravimetric snow-density measurements of SWE depth (SWE$_{\mathrm{m}}$) and snow depth (H) (Eq. 15). The R^2 value relating the DEID and manual bulk-density measurements is 0.88 with a slope 0.90 ± 0.15, as shown in Fig. 11. The implication of these two comparisons, somewhat surprisingly, is that the DEID reproduces measurements made with more traditional techniques of freshly fallen snowpack density and accumulation
370   without considering the quite complex physics of how individual snowflakes pack and stack.

5   Conclusions

Automated determination of the density of individual snowflakes has been a long-standing challenge. In this study, we present a novel method for accomplishing this goal that exploits a new hotplate instrument, the Differential Emissivity Imaging Disdrometer or DEID, which has previously been shown capable of obtaining highly accurate direct measurements of particle
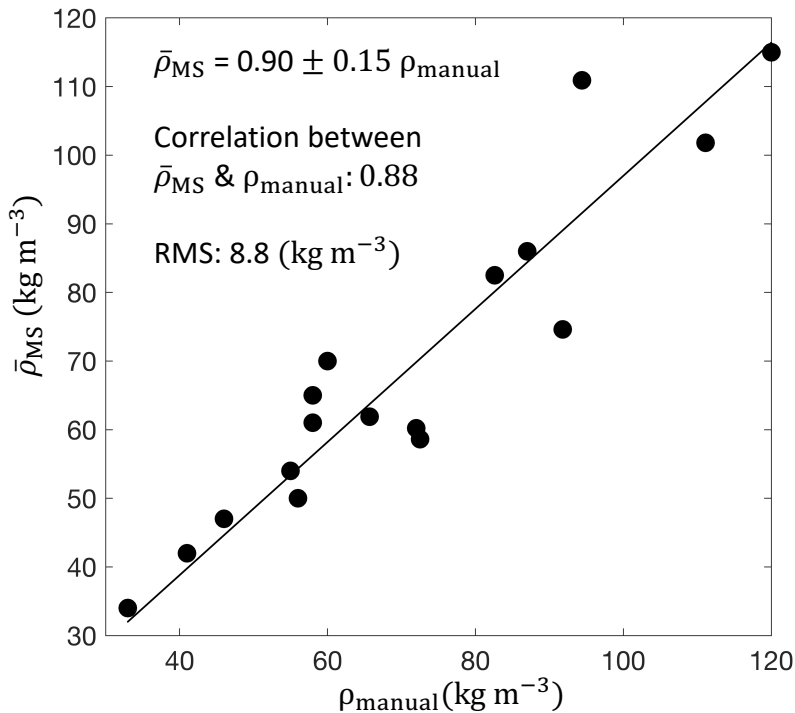
Figure 11. For seventeen storms, comparison between bulk density of snowpack from the DEID obtained using the MS density method and from manual gravimetric snow-density measurements made every 12 hours (1100 UTC and 2300 UTC). Each data point represents a storm.

mass. Particle-by-particle density estimates are obtained from measurements of particle mass, particle projected area onto the hotplate, and an estimate of the particle thickness using melting speed and melting time. A particle's thickness normal to the hotplate is a product of the melting speed and melting time from which, in combination with a particle's area, an estimate can be obtained of particle volume and hence its density. For individual hydrometeors, this 'melting-speed method' was validated using laboratory ice particles of known density showing a maximum uncertainty of 6.3%, as well as with videos from field measurements of a range of natural falling snowflakes with an uncertainty of 3.7%. DEID observations at a high elevation mountain site of snow water equivalent (SWE) accumulation, snow depth accumulation (H), and bulk snow density ($\bar{\rho}_{MS}$) from seventeen storms taken at the Alta-Collins snow-study plot at Alta Ski Area during winter 2020-2021 agreed well with traditional manual techniques measurements with R^2 values of 0.994, 0.983 and 0.88, with slope 0.94 ± 0.04, 1.12 ± 0.07 and 0.90 ± 0.15, respectively independent of environmental conditions, including wind speed, ambient temperature, relative humidity, and hotplate temperature.

Using the melting-speed method, the utility of the DEID design can be extended from hydrometeor mass measurement to measurement of the density of irregularly shaped hydrometeors, in real-time with high accuracy. Such information, whether taken on a particle-by-particle basis or assessed as a cumulative bulk quantity has applications for high-resolution measurement of vertical density variability in the snowpack (e.g., Morrison et al. (2023))– critical for assessment of its stability – as well as
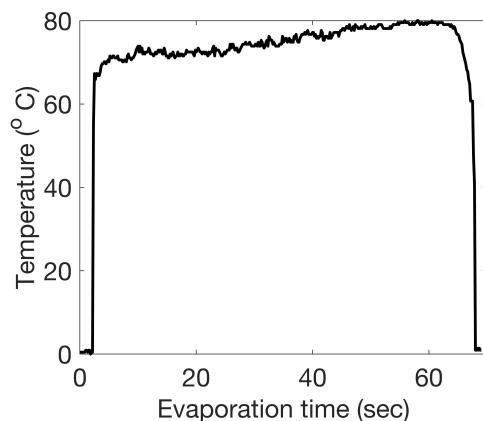
Figure A1. Sample time series of the temperature of the melted portion of an ice particle after being placed on the hotplate. A 60 μL water droplet volume was used to make the ice particle shown here.

390 for studies of snow metamorphism, assessment of transitions between rain and snow, determinations of rates of hydrometeor settling and its response to turbulence, and the scattering by snow particles of visible light and radar pulses.

Code availability. The data processing codes are protected through a patent and are not available for distribution. The codes used for processing follow the methodologies and equations described herein.

Data availability. Data from the ETI Noah II precipitation gauge and ultrasonic snow-depth are openly accessible from https://mesowest.utah.edu
395 (University of Utah, 2021), Station ID: CLN. All other datasets are available upon request.

Appendix A: Latent heat of evaporation calculation

The latent heat of vaporization of water depends on temperature and may be written as $L_v(T) = (2.501 - 0.00237 \times T) \times 10^6$ J kg^{-1}, where T is in degrees Celsius (Stull (2012)). In our case, water droplets evaporate at temperatures from 0 to 85 °C. A sample time series of the temperature of a water droplet during evaporation is plotted in Fig. A1. The estimated L_v based on
400 the time series of temperature of water droplets is $2.32 \pm 0.02 \times 10^6$ Jkg^{-1}.

Appendix B: Relation between the melting and evaporation statistics

Using Eq. (2), the mass associated with each pixel can be estimated separately during melting and evaporation as shown in Eqs. (B1) and (B2) below, respectively.

$$m = \frac{\kappa}{C_{\mathrm{ice}}T_0 + L_f} \int_0^{\Delta t_{\mathrm{melt}}} \Delta T_{melt}(t) A(t) \, dt \tag{B1}$$

405

$$m = \frac{\kappa}{C_{\mathrm{liq}}T_p + L_v} \int_0^{\Delta t_{\mathrm{evap}}} \Delta T_{evap}(t) A(t) \, dt \tag{B2}$$

By using Eq. (B1) and Eq. (B2) and applying an averaging approximation, we may write

$$\frac{\Delta T_{\mathrm{melt}} \Delta t_{\mathrm{melt}}}{L_{ff}} \approx \frac{\Delta T_{\mathrm{evap}} \Delta t_{\mathrm{evap}}}{L_{vv}}. \tag{B3}$$

Here, $L_{ff} = C_{\mathrm{ice}}T_0 + L_f$ and $L_{vv} = C_{\mathrm{liq}}T_p + L_v$

410   Experimentally determined values for ΔT_{melt}, Δt_{melt}, ΔT_{evap} and Δt_{evap} for different ice-particle masses and sizes for a large range of environmental conditions are shown in Fig. B1. As expected, the slope between the two-terms agrees to within 6.5% of the ratio of L_{vv} to L_{ff}. With the DEID, Δt_{melt} and Δt_{evap} are directly measured using a thermal camera and counting the number of frames between the first frame when an ice particle hits the hotplate and last frame when the particle has completely melted or evaporated.

Appendix C: DEID Thermal Imagery

415

In this section, we present example thermal images of different types of snowflakes after melting and during evaporation on the DEID hotplate. Figures C1 and C2 show aggregate and graupel snow particles, respectively. These data were taken at the Alta-Collins snow-study plot on 22 December 2020.

Appendix D: Systematic and Random error analysis

420   Direct measurements made by the DEID include snowflake area, temperature, and evaporation time, for which the respective uncertainties are 1.4%, 0.3%, and 1.6%. Due to the inclination of the thermal camera, the maximum error in the measurement of area is 1.6%, and it is corrected using a custom-made Matlab function based on the height and angle of the thermal camera. Both x and y direction pixels were corrected using algorithm $h_{\mathrm{cam}} \tan(\theta_y + j d\theta)$. Here, h_{cam} is the height of the camera and $\theta_y = 90 - \theta_H - \theta_V/2$. The angles θ_H and θ_V are the thermal camera's horizontal and vertical angles, $d\theta$ is, θ_V/j, where j

425   is the number of pixels in y-direction. A similar method was used for the x direction. The uncertainties in derived quantities
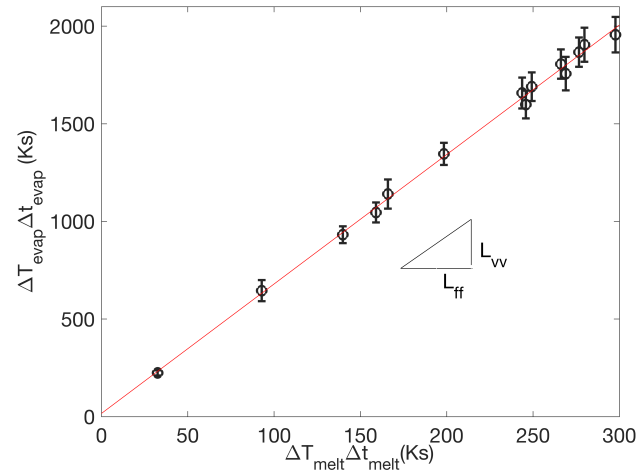
Figure B1. Experimentally measured Δt_{melt}, ΔT_{melt}, Δt_{evap} and ΔT_{evap} for laboratory ice particles. The slope of the line is quite close to L_{vv}/L_{ff}. An error bar is associated with ten samples in each ice particle size.
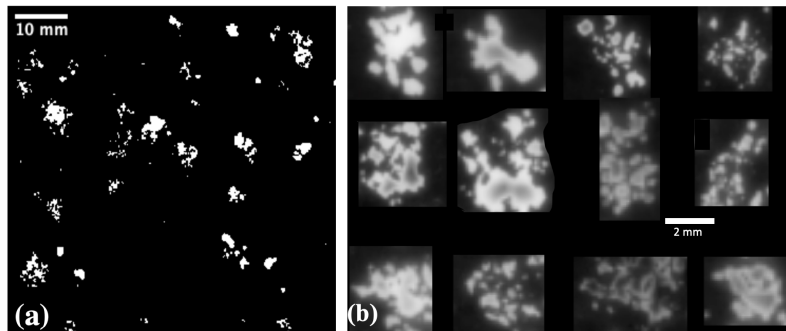
Figure C1. (a)Black and white binary thermal images of an aggregate type of snowflakes at different stages of melting and evaporation on the DEID hotplate observed in Alta, UT. (b) Cropped aggregate snowflake images on the hotplate just after melting.
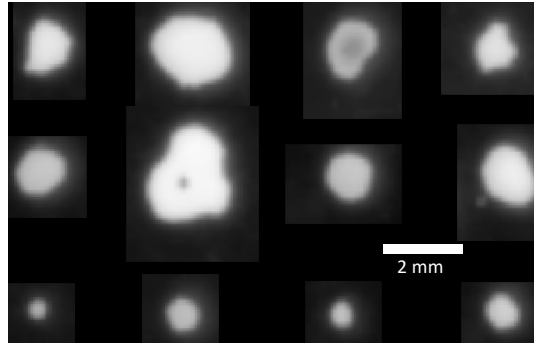
Figure C2. Black and white binary thermal images of graupel type of snowflakes in different stages of melting and evaporation on the DEID heated plate observed at Alta.

(using a standard propagation of uncertainty analysis) such as mass (m), height (h) and density (ρ_s), are 4.3%, 2.9% and 8.6%, respectively.

Author contributions. D.K.S., E.R.P. and T.J.G. designed the experiments and D.K.S performed the experiments in consultation with E.R.P and T.J.G.; All authors analyzed the data and contributed to writing and editing the paper.

430 *Competing interests.* Conflict of interest: The DEID technology is protected through patent US20210172855A1 co-authored with D.K.S., E.R.P., and T.J.G. and is commercially available through Particle Flux Analytics, Inc. T.J.G. is a co-owner of Particle Flux Analytics, Inc. which has a license from the University of Utah to commercialize the DEID.

Acknowledgements. We thank Allan Reaburn and his colleagues at Particle Flux Analytics, Inc. for their contributions to the development of the DEID, Dave Richards, Jonathan Morgan, and the Alta Ski Patrol for field support, and Spencer Donovan for contributions to the
435 experimental setup. This work was supported by the U.S. National Science Foundation through the following grants: PDM-1841870 and PDM-2210179)

References

Alcott, T. I. and Steenburgh, W. J.: Snow-to-liquid ratio variability and prediction at a high-elevation site in Utah's Wasatch Mountains, Weather. Forecast., 25, 323–337, 2010.

Dickinson, R. E.: Land surface processes and climate—Surface albedos and energy balance, in: Advances in geophysics, vol. 25, pp. 305–353, Elsevier, 1983.

Dunnavan, E. L., Jiang, Z., Harrington, J. Y., Verlinde, J., Fitch, K., and Garrett, T. J.: The shape and density evolution of snow aggregates, Journal of the Atmospheric Sciences, 76, 3919–3940, 2019.

Fierz, C., Armstrong, R. L., Durand, Y., Etchevers, P., Greene, E., McClung, D. M., Nishimura, K., Satyawali, P. K., and Sokratov, S. A.: The international classification for seasonal snow on the ground, UNESCO, 2009.

Finlon, J. A., McFarquhar, G. M., Nesbitt, S. W., Rauber, R. M., Morrison, H., Wu, W., and Zhang, P.: A novel approach for characterizing the variability in mass–dimension relationships: results from MC3E, Atmos. Chem. Phys., 19, 3621–3643, 2019.

Fovell, R. G. and Su, H.: Impact of cloud microphysics on hurricane track forecasts, Geophys. Res. Lett., 34, L24 810, 2007.

Gergely, M., Schneebeli, M., and Roth, K.: First experiments to determine snow density from diffuse near-infrared transmittance, Cold regions science and technology, 64, 81–86, 2010.

Hong, S.-Y., Dudhia, J., and Chen, S.-H.: A revised approach to ice microphysical processes for the bulk parameterization of clouds and precipitation, Mon. Wea. Rev., 132, 103–120, 2004.

Kendra, J. R., Ulaby, F. T., and Sarabandi, K.: Snow probe for in situ determination of wetness and density, IEEE transactions on geoscience and remote sensing, 32, 1152–1159, 1994.

Kokhanovsky, A. A. and Zege, E. P.: Scattering optics of snow, Applied optics, 43, 1589–1602, 2004.

Kosky, P., Balmer, R., Keat, W., and Wise, G.: Exploring engineering 3rd edition, Book, pp. 451–462, 2013.

Li, J., Guala, M., and Hong, J.: Snow particle analyzer for simultaneous measurements of snow density and morphology, arXiv preprint arXiv:2209.11129, 2022.

Morrison, T. J., Meisenheimer, T., Garrett, T., Singh, D., Donovan, S., and Pardyjak, E.: Relating storm-snow avalanche instabilities to data collected from the Differential Emissivity Imaging Disdrometer (DEID), Cold Regions Science and Technology, accepted for publication, 2023.

Praz, C., Roulet, Y.-A., and Berne, A.: Solid hydrometeor classification and riming degree estimation from pictures collected with a Multi-Angle Snowflake Camera, Atmospheric Measurement Techniques, 10, 1335–1357, 2017.

Proksch, M., Rutter, N., Fierz, C., and Schneebeli, M.: Intercomparison of snow density measurements: bias, precision, and vertical resolution, The Cryosphere, 10, 371–384, 2016.

Rango, A. and Martinec, J.: Revisiting the degree-day method for snowmelt computations 1, JAWRA Journal of the American Water Resources Association, 31, 657–669, 1995.

Rasmussen, R. M., Hallett, R., and Purcell, J.: The hotplate precipitation gauge, J. Atmos. Ocean. Tech., 28, 148–164, 2011.

Rees, K. N. and Garrett, T. J.: Idealized simulation study of the relationship of disdrometer sampling statistics with the precision of precipitation rate measurement, Atmospheric Measurement Techniques, 14, 7681–7691, 2021.

Rees, K. N., Singh, D. K., Pardyjak, E. R., and Garrett, T. J.: Mass and density of individual frozen hydrometeors, Atmos. Chem. Phys., 21, 14 235–14 250, 2021.

Rutledge, S. A. and Hobbs, P. V.: The mesoscale and microscale structure and organization of clouds and precipitation in midlatitude cyclones. XII: A diagnostic modeling study of precipitation development in narrow cold-frontal rainbands., J. Atmos. Sci., 41, 2949–2972, 1984.

475 Schweizer, J., van Herwijnen, A., and Reuter, B.: Measurements of weak layer fracture energy, Cold Regions Science and Technology, 69, 139–144, 2011.

Singh, D. K., Donovan, S., Pardyjak, E. R., and Garrett, T. J.: A differential emissivity imaging technique for measuring hydrometeor mass and type, Atmos. Meas. Tech., 14, 6973–6990, 2021.

Stull, R. B.: An introduction to boundary layer meteorology, vol. 13, Springer Science & Business Media, 2012.

480 Sturm, M., Taras, B., Liston, G. E., Derksen, C., Jonas, T., and Lea, J.: Estimating snow water equivalent using snow depth data and climate classes, Journal of Hydrometeorology, 11, 1380–1394, 2010.

Tiira, J., Moisseev, D. N., Von Lerber, A., Ori, D., Tokay, A., Bliven, L. F., and Petersen, W.: Ensemble mean density and its connection to other microphysical properties of falling snow as observed in Southern Finland, Atmospheric Measurement Techniques, 9, 4825–4841, 2016.